Rare Met. (2016) 35(7):551–558
DOI 10.1007/s12598-015-0465-x

RARE METALS
www.editorialmanager.com/rmet

Magnetoresistive properties of Ni-doped $La_{0.7}Sr_{0.3}MnO_3$ manganites

Ahmed Mohamed Ahmed, Abd El-Moez Ahmed Mohamed*, Medhat Abdelrady Abdellateef, Hassan Ahmed Abd El-Ghanny

Received: 30 November 2014 / Revised: 16 January 2015 / Accepted: 28 February 2015 / Published online: 24 March 2015

Abstract $La_{0.7}Sr_{0.3}Mn_{1-x}Ni_xO_3$ ($x = 0$, 0.025, 0.050 and 0.075) ceramics were prepared by the conventional solid-state reaction method. The partial substitution of Mn by Ni^{2+} leads to a decrease in cell volume as well as a structural transition from the rhombohedral to the orthorhombic structure. Ni^{2+} doping increases the electrical resistivity, decreases the semiconductor–metal transition temperature (T_{ms}) and relatively enhances the room temperature magnetoresistance (MR), especially in $x = 0.025$ and around T_{ms}. With respect to conduction mechanism, the small polaron hopping (SPH) and the variable range hopping (VRH) models were used to examine conduction in the semiconducting region.

Keywords Manganites; X-ray diffraction; Structure; Electrical resistivity; Magnetoresistance

1 Introduction

Perovskite $A_{1-x}B_xMnO_3$ manganites (where A is a rare earth element as La^{3+}, Nd^{3+}, etc., and B is a divalent cation as Sr^{2+}, Ca^{2+}, Ba^{2+}, etc.) draw a lot of attention because of its properties. Its importance does not refer only to its elastic [1], structural, electronic and magnetic transition [2] properties, but also to the fascinating colossal magnetoresistance (CMR) property, which makes them an important material for applications [3, 4]. These properties can be controlled by several factors as the preparation method, the divalent ion content and size. CMR was explained on the basis of double exchange (DE) interaction, super-exchange interaction, charge localization via Jahn–Teller distortion with polaron formation, phase separation and site disorder; however, there are some complexities in the theoretical explanation. Among these materials, $La_{1-x}Sr_xMnO_3$ is the most interested compounds, especially $La_{0.7}Sr_{0.3}MnO_3$ due to its large ferromagnetic ordering temperature (T_c) [5], besides to the exploration of $x = 0.1$–0.3 series as solid oxides fuel cell materials [6, 7].

Moreover, substitution of Mn ion by other transition metals such as Ni, Fe or Co is an interesting topic that attracts researchers to study [8, 9]. This substitution results in a disturbance in Mn^{3+}–O–Mn^{4+} chains, leading to a change in Mn^{3+}/Mn^{4+} ratio and destroying its coupling. This appears as a weakness in ferromagnetism, a change in transport properties [10], an increase in CMR effect [11] and a decrease in semiconductor–metal transition temperature (T_{ms}) (but it depends on the doping element) [12]. Ni^{2+} is an interesting transition metal for Mn-site substitution, where the combination of Ni^{2+} with Mn^{4+} is favorable [13, 14]; but from the previous works, it weakens ferromagnetism [15, 16], which has a relation with DE reduction [17]. Nickel manganites oxides are considered as very good negative temperature coefficient (NTC) thermistors [18], and during the magnetoresistance (MR) it can be useful in magnetic applications. But for applications, in general, high MR values in small applied magnetic fields over a wide range of temperature are desirable [19], known as low field magnetoresistance (LFMR). Thus, the aim of this work is to investigate the structural, electrical and magnetoresistive properties of the polycrystalline $La_{0.7}Sr_{0.3}Mn_{1-x}Ni_xO_3$ for LFMR applications.

2 Experimental

The $La_{0.7}Sr_{0.3}Mn_{1-x}Ni_xO_3$ ceramics with $x = 0$, 0.025, 0.050 and 0.075 were prepared by the conventional solid-state

A. M. Ahmed, A. E.-M. A. Mohamed*, M. A. Abdellateef, H. A. Abd El-Ghanny
Physics Department, Faculty of Science, Sohag University, Sohâg 82524, Egypt
e-mail: abdmoez_hussien@science.sohag.edu.eg

reaction method. The starting raw La_2O_3, $SrCO_3$, $MnCO_3$ and NiO were mixed in stoichiometric proportions; La_2O_3 was dehydrated at 600 °C for 6 h. The mixture was ground for 6 h to ensure homogeneity and pressed into pellets under 490 MPa. The pellets were calcined in air at 900 °C for 10 h, and then they were reground for 5 h and pressed again under higher pressure of 980 MPa. They were sintered at 1100 °C for 20 h and left to cool gradually to room temperature. The electrical measurements were carried out by the standard four-point Van der Pauw technique in the temperature range of 80–290 K and at magnetic field of 0 and 0.5 T. All samples were examined by X-ray diffraction (XRD) with Cu Kα and wavelength of 0.15406 nm in angle range (2θ) of 18.00°–99.99°. The crystal structure and the lattice parameters were refined by Rietveld method using FULLPROF program.

3 Results and discussion

3.1 Structure

The XRD patterns in Fig. 1 show that all samples possess single phase with some additional diffraction peaks of La_2O_3 around $2\theta = 27°$ disappearing with doping. The same peaks were also observed by Wandekar et al. [20, 21] in Co- and Ni-doped La–Sr–Mn–O systems. These peaks can be observed in $La_{1-x}Sr_xMnO_3$ system at $x \geq 0.3$ [22] because of the incomplete reaction between elements. Thus, Ni^{2+} addition may enhance the reaction between elements due to its bigger ionic size compared with Mn and decrease La_2O_3 peak's intensity. Rietveld refinement of the patterns shows that the parent $La_{0.7}Sr_{0.3}MnO_3$ (LSMO) crystallizes in the *R*-3*C* rhombohedral structure and gradually distorts to the orthorhombic structure with Ni^{2+} content up to $x = 0.050$, while for $x = 0.075$ it has a complete orthorhombic (*Pbnm*) structure (Table 1). The orthorhombic symmetry and structural transition were reported previously by Joshi and Hu et al. [23, 24], respectively. Mn/Ni atoms were refined at (0, 0, 0) site, and the agreement factors of refinement are shown in Table 1 as Bragg factor (R_B) and goodness of fitting (χ^2). The average particle size was calculated from XRD using Laue–Scherrer's formula and is presented in Table 1, which decreases with Ni^{2+} content increasing.

The structural transition proves the success of Ni^{2+} in the substitution process, which can be emphasized by the relative change in both lattice parameters and cell volume with Ni^{2+} content (Table 1). In spite of the larger ionic size of Ni^{2+} compared with Mn^{3+} [21] and Mn^{4+} (Ni^{2+}, 0.069 nm; Mn^{3+}, 0.066 nm; Mn^{4+}, 0.060 nm), lattice parameters (*a*, *b*, *c*) and cell volume decrease with Ni^{2+} content, which is in agreement with the results in Refs. [25–27], and this decrease is large for $x = 0.075$. This suggests that either oxygen vacancies are created or charge balance by converting Mn^{3+} to Mn^{4+} may occur with Ni^{2+} content. But, in the later case, cell parameters are not expected to change much. So, it is more probable that oxygen vacancies were created and resulted in the reduction of cell volume [20, 25].

3.2 Electrical properties

Figure 2 shows the curves of temperature (*T*) dependence of resistivity (ρ) where an increase in resistivity and a decrease in T_{ms} are observed with doping. The metallic state below T_{ms} can be described on the basis of the DE mechanism (Mn^{3+}–O–Mn^{4+}) [5] that will be used to understand the increase in resistivity and the decrease in T_{ms} (Table 2). As Mn ions are partially substituted by Ni^{2+}, the change in Mn^{3+}/Mn^{4+} ratio produces a decrease in DE, demonstrating the decrease in T_{ms}. In other words, Ni^{2+} doping suppresses DE because of its non-participation in this mechanism (Mn^{3+}–O–Ni^{2+}). This can be clarified by considering that many bonds may form as the ferromagnetic Mn^{4+}–O–Ni^{2+}

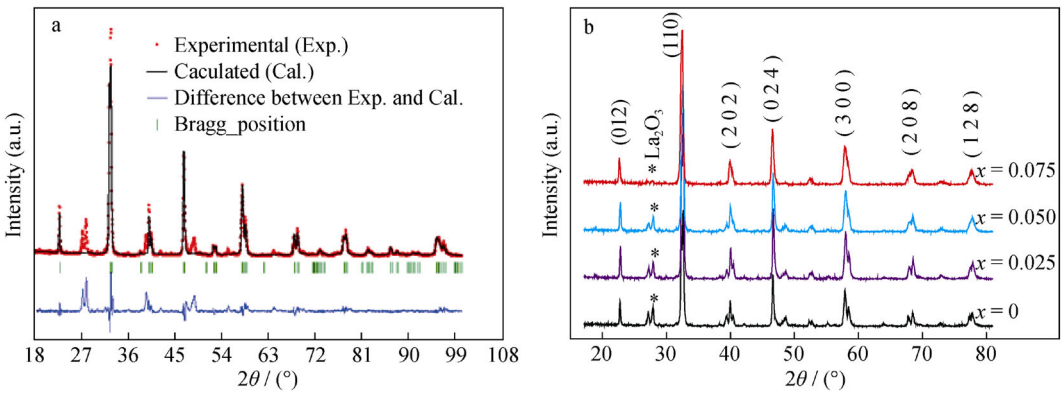

Fig. 1 **a** Rietveld-based calculated profile of $La_{0.7}Sr_{0.3}Mn_{0.925}Ni_{0.075}O_3$ at room temperature and **b** XRD patterns of $La_{0.7}Sr_{0.3}Mn_{1-x}Ni_xO_3$ ($x = 0$, 0.025, 0.050 and 0.075)

Table 1 Phase symmetry, lattice parameters, cell volume, average particle size by XRD and agreement factors of $La_{0.7}Sr_{0.3}Mn_{1-x}Ni_xO_3$ compounds

x	Phase symmetry	a/nm	b/nm	c/nm	Cell volume/nm^3	R_B/%	χ^2	Average particle size/nm
0	*R*-3*C*	0.5519	0.5519	1.3350	0.352201	4.18	5.7	24
0.025	*R*-3*C*	0.5516	0.5516	1.3346	0.351124	6.98	5.2	21
0.050	*R*-3*C*	0.5510	0.5510	1.3343	0.350927	7.47	4.1	20
0.075	*Pbnm*	0.5449	0.5514	0.7751	0.233011	6.69	3.6	17

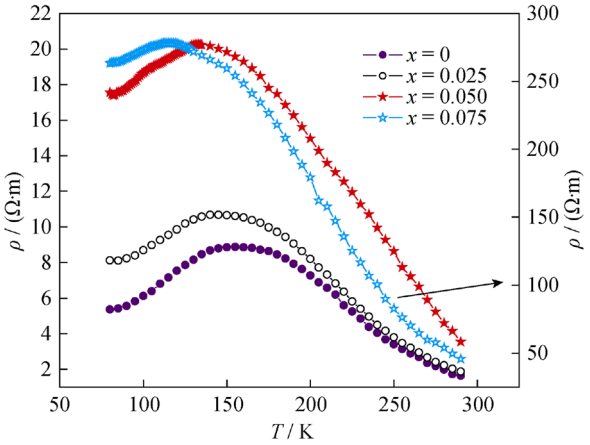

Fig. 2 Temperature dependence of resistivity, ρ (T), of $La_{0.7}Sr_{0.3}Mn_{1-x}Ni_xO_3$ compounds

bonds that can increase ferromagnetism and so T_{ms}. But, as we can see from Fig. 2 and Table 2, there is a decrease in metallic region and T_{ms}, which means the impossibility of these bonds formation [28]. But Ni^{2+} may be surrounded by the same ions consisting Ni^{2+}–O–Ni^{2+} bonds and so Mn^{4+} consisting Mn^{4+}–O–Mn^{4+} bonds, coupling antiferromagnetically and weakening DE [26, 28–30]. These antiferromagnetic bonds may increase in number with Ni^{2+} content, and this is a logical scenario, explaining T_{ms} decreases and resistivity increases.

With DE decreasing, the e_g band electron of Mn encounters a difficulty in wandering that results in the increase of resistivity (Fig. 2). As shown in Fig. 2, the parent compound LSMO has a smaller resistivity compared with the doped samples, which is in agreement with the result in Ref. [25]. This increase in resistivity with Ni^{2+} ratio increasing can be explained also in terms of the change in Mn ions angle. Mn–O–Mn angle (θ) plays an important role in the e_g electron mobility, where deviation from 180° increases distortion, decreases the transfer integral (t), $t = t_0\cos(\theta/2)$ (where t_0 is the maximum value of t), decreases the DE [31] between Mn ions and increases resistivity. Thus, it is easy for conduction electron to move in the rhombohedral structure rather than the orthorhombic structure that has high bond distortion, resulting in localized carriers and higher resistivity. This may be clear from our results that during the gradual increase in resistivity with the gradual orthorhombic distortion with doping (up to $x = 0.050$), and the abrupt increase in resistivity associated with the complete orthorhombic distortion in $x = 0.075$, this abrupt increase in resistivity agrees with the orthorhombic phase of $La_{0.7}Sr_{0.3}Mn_{1-x}Fe_xO_3$ [32].

The thermal variation of resistivity measured in applied magnetic field (H) of 0.5 T is presented in Fig. 3. For each sample, the isothermal resistivity values measured in $H = 0.5$ T are lower than that measured in $H = 0$ T. In addition, T_{ms} values do not change under the effect of magnetic field except in $x = 0.075$ where there is a slight increase in its value (Table 2). This decrease in resistivity is due to the oriented spins by the applied magnetic field that eliminates charge carrier scattering during hopping process. Note that T_{ms} values tabulated in Table 2 are far below room temperature, which can be attributed to the small particle size [33] that can decrease bond angle and increase its length [34], leading to a decrease in the transfer integral which in turn decreases T_{ms} and increases resistivity.

Table 2 T_{ms} at magnetic field of 0 and 0.5 T, Debye temperature, θ_D, phonon frequency, υ_{ph}, E_ρ, $N(E_F)$, W_H and W_D of $La_{0.7}Sr_{0.3}Mn_{1-x}Ni_xO_3$ compounds

x	$T_{ms(0\ T)}$/K	$T_{ms(0.5\ T)}$/K	θ_D/K	υ_{ph}/10^{12}Hz	E_ρ/meV	$N(E_F)$/(10^{20}eV^{-1}·cm^{-3})	W_H/meV	W_D/meV
0	155	155	439.0	9.15	109.313	47.51	108.27	2.07
0.025	145	145	479.9	10.00	141.014	17.34	139.47	3.08
0.050	131	131	509.9	10.61	180.093	16.57	177.32	5.54
0.075	116	120	440.0	9.17	112.603	12.57	109.81	5.56

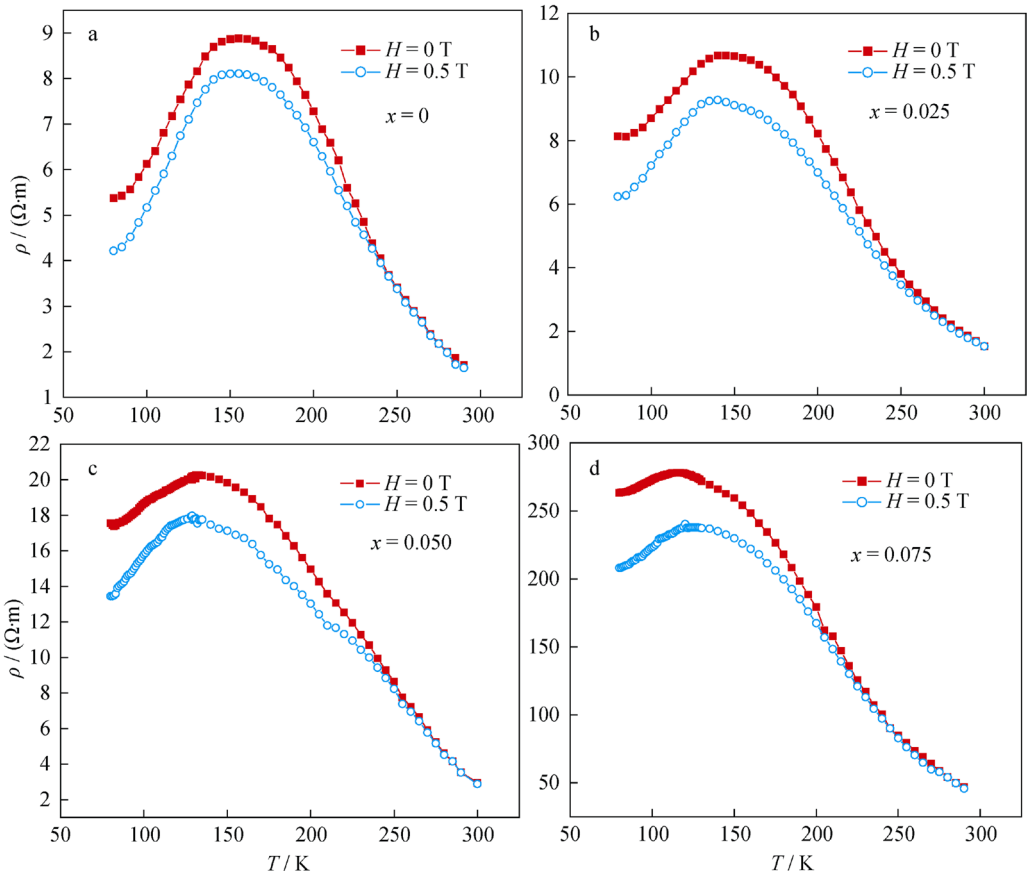

Fig. 3 Thermal variation of resistivity in $H = 0$ T and $H = 0.5$ T of $La_{0.7}Sr_{0.3}Mn_{1-x}Ni_xO_3$ compounds: **a** $x = 0$, **b** $x = 0.025$, **c** $x = 0.050$, and **d** $x = 0.075$

3.3 Magnetoresistance (MR)

Magnetoresistance was calculated from $[\rho(H) - \rho(0)]/\rho(0)$, where $\rho(H)$ is the resistivity measured in $H = 0.5$ T and $\rho(0)$ is the resistivity measured in $H = 0$ T. Figure 4 shows the temperature dependence of MR. The negative values of MR indicate that the resistivity is affected by the applied magnetic field. The highest MR values are observed at low temperatures, which may be due to the spin dependent transport at grain boundaries [35–37]. With temperature elevating, MR decreases passing through broad hump at $T > T_{ms}$ except $x = 0.075$. At hump, MR increases in $x = 0.025$ and then decreases with further doping. For the first two doping samples, $x = 0.025$ and $x = 0.050$, the MR broad hump is enhanced and has a larger value compared with the parent LSMO compound.

The MR values at room temperature (290 K) for samples are shown in Fig. 5, the highest value is observed for $x = 0.025$ and decreases at higher doping contents of $x = 0.050$ and 0.075. The room temperature MR values for all samples are −0.13 %, −4.26 %, −0.86 % and −0.73 % for $x = 0$, 0.025, 0.050 and 0.075, respectively; thus, Ni^{2+}

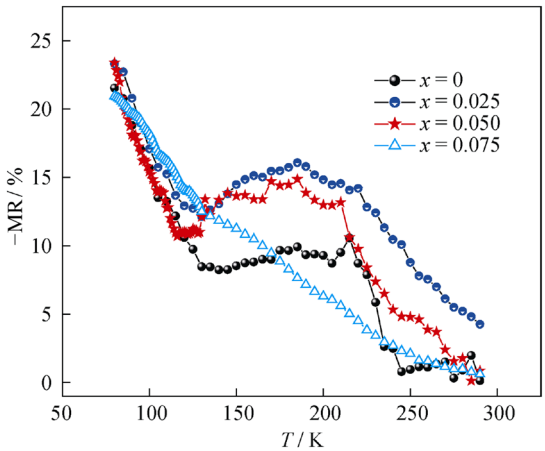

Fig. 4 Temperature dependence of MR of $La_{0.7}Sr_{0.3}Mn_{1-x}Ni_xO_3$ compounds

doping can help electron transition rather than LSMO. This promotion in MR was observed in polycrystalline materials [38] and correlated to the spin dependant tunneling and the scattering process at grain boundaries. At grain boundaries, magnetization in grains is no longer oriented or connected,

so carriers have to cross grains in tunneling. So, MR enhancement is related to the improvement of oriented states at grain boundaries. Consequently, we can expect that, at low doping level, the number of oriented states at grain boundaries is greater than that in LSMO. While, at high doping level, the disoriented states become higher and the thickness of grain boundaries may make the electron tunneling more difficult [27], which may decrease MR.

3.4 Conduction mechanisms above and below T_{ms}

In the semiconducting region ($T > T_{ms}$), a lot of works discussed the existence of variable range hopping (VRH) [39–41] as the only mechanism that governs the variation of electrical resistivity with temperature. But many articles proved the presence of polaron in the same region [42, 43]. Resistivity data at $T > T_{ms}$ are well fitted with Mott and Davis small polaron hopping (SPH) model [44] above $T > \theta_D/2$ with the following expression:

$$\rho/T = \rho_\alpha \exp\left(E_\rho/k_B T\right) \quad (1)$$

$$\rho_\alpha = \left[k_B/\upsilon_{ph} N e^2 R^2 C(1-C)\ \exp(2\alpha R)\right] \quad (2)$$

where $\theta_D/2$ is the deviation temperature of linearity, θ_D is Debye temperature, and Fig. 6a is SPH example of LSMO, k_B is the Boltzmann constant, T is the absolute temperature, N is the number of ion sites per unit volume, R is the average inter-site spacing, C is the fraction of sites occupied by a polaron, α is the electron wave function decay constant, υ_{ph} is the optical phonon frequency (estimated from $h\upsilon_{ph} = k_B\theta_D$ relation) and E_ρ is the sum of the activation energy required to create free carriers (disorder energy) and the energy that activates carriers for hopping.

$$E_\rho = \begin{cases} W_H + W_D/2 & \text{for } T > \theta_D/2 \\ W_D & \text{for } T < \theta_D/4 \end{cases} \quad (3)$$

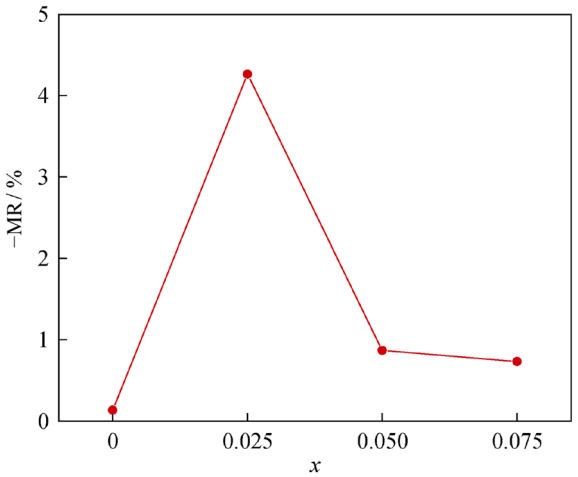

Fig. 5 MR versus Ni^{2+} content (x) at room temperature (290 K)

where W_D is the disorder energy and W_H is the polaron hopping energy which is the difference between the electric activation energy (E_ρ) and the thermoelectric activation energy (E_s) ($W_H = E_\rho - E_s$) [8].

The values of θ_D, E_ρ, $N(E_F)$, υ_{ph}, W_H and W_D were calculated and are tabulated in Table 2. Generally, all of these parameters increase with Ni^{2+} content (except $x = 0.075$) due to e_g electron localization, while W_D increases even in $x = 0.075$. The increase in E_ρ can be explained by the electron–phonon interaction that results in carrier's localization. So the energy required to create free carriers increases. For more accuracy, small polaron coupling interaction (γ_{ph}), which is a measurement of electron–phonon interaction, was calculated from the following relation [43] as shown in Table 3:

$$\gamma_{ph} = 2W_H/h\upsilon_{ph} \quad (4)$$

where γ_{ph} increases with Ni^{2+} content, asserting the previous explanation. According to Austin and Mott [45], the strong electron–phonon interaction can occur as the value of γ_{ph} goes up to 4 ($\gamma_{ph} > 4$), which is in a good agreement with the present results (Table 3). Also, the polaron mass (m_p) and the effective rigid mass of lattice (m^*) are related in the relation:

$$m_p = m^* \exp\left(\gamma_{ph}\right) \quad (5)$$

where $\exp(\gamma_{ph})$ in Table 3 has high values, confirming the strong electron–phonon interaction [46].

As stated before, only VRH cannot describe the whole semiconducting range, but it is dominant in part of it. ρ (T) curves are found to be fitted well with VRH model in the temperature range of $T_{ms} < T < \theta_D/2$ [47], as shown in Fig. 6b for LSMO as an example, obeying the following expression [8]:

$$\sigma = \sigma_0 \exp\left(-T_0/T\right)^{1/4} \quad (6)$$

where T_0 is a constant (Mott characteristic temperature):

$$T_0 = 18/k_B N(E_F) a^3 \quad (7)$$

where $N(E_F)$ is the density of states near Fermi level (E_F) and a is the localization length equals to 0.45 nm reported by Viret et al. [48]. The observed decrease in $N(E_F)$ with Ni^{2+} content in Table 2 may refer to the carriers' localization and the increase in resistivity.

To determine whether the polaron hopping conduction is adiabatic or non-adiabatic process, Holstein conditions were used [49]. According to these criteria, polaron band width (J) should satisfy one of these conditions: $J > P$ for adiabatic condition; $J < P$ for non-adiabatic condition

$$J(T) \approx 0.67 h\upsilon_{ph}(T/\theta_D)^{1/4} \quad (8)$$

$$P(T) = (2k_B T W_H/\pi)^{1/4}\left(h\upsilon_{ph}/\pi\right)^{1/2} \quad (9)$$

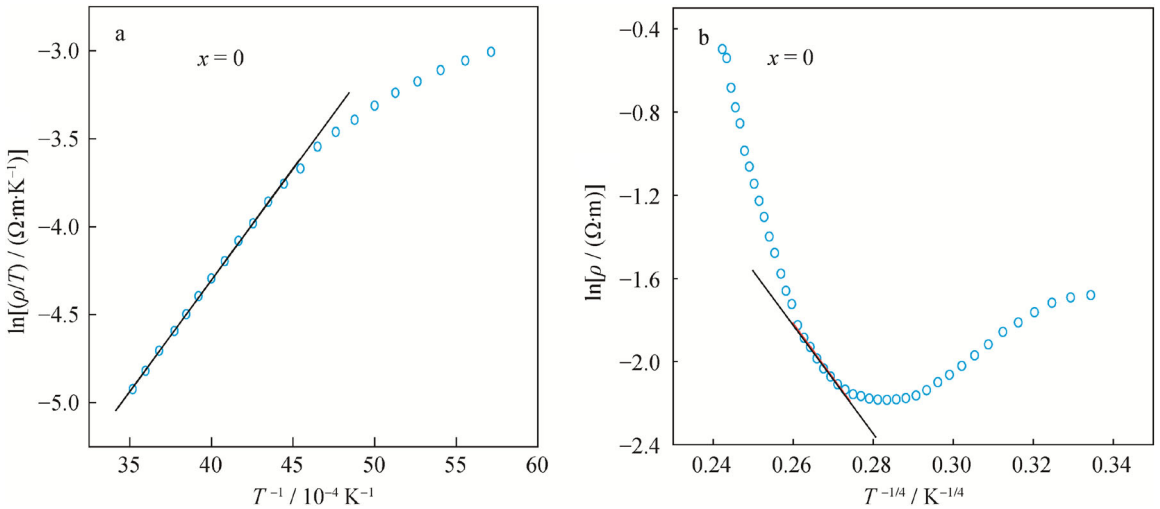

Fig. 6 **a** SPH and **b** VRH models of parent LSMO in $H = 0$ T, solid line representing the best fitted points with these models

Table 3 P, J, γ_{ph}, exp (γ_{ph}) and $W_H/3$ parameters of $La_{0.7}Sr_{0.3}Mn_{1-x}Ni_xO_3$ compounds at (290 K)

x	P/meV	J/meV	γ_{ph}	exp(γ_{ph})	$W_H/3$/meV
0	22.34	22.80	5.73	309.95	36.09
0.025	24.89	24.38	6.75	861.15	46.49
0.050	27.21	25.47	8.10	3303.21	59.10
0.075	22.45	22.84	5.80	331.98	36.60

Results in Table 3 prove the small polaron formation since it can be formed under the condition of $J < W_H/3$ [49], confirming SPH conduction at high temperatures. For LSMO, $J > P$ means that the system is in the adiabatic state, but with Ni^{2+} doping content up to $x = 0.050$, the system converts to the non-adiabatic state ($J < P$). However, with Ni^{2+}doping content further increasing ($x = 0.075$), the system returns back to the adiabatic state (Table 3). The important conclusion drawn is that a small amount of Ni^{2+} (up to 0.050) can convert LSMO system from adiabatic to non-adiabatic state.

Resistivity data below T_{ms} were examined by empirical equations to know the nature of conduction at low temperatures.

$$\rho = \rho_0 + \rho_2 T^2 \quad (10)$$

$$\rho = \rho_0 + \rho_{2.5} T^{2.5} \quad (11)$$

$$\rho = \rho_0 + \rho_2 T^2 + \rho_{4.5} T^{4.5} \quad (12)$$

$$\rho = \rho_0 + \rho_2 T^2 + \rho_{4.5} T^{4.5} + \rho_5 T^5 \quad (13)$$

where ρ_0 is the resistivity term arising due to domains, grain boundaries and temperature independent process [50], $\rho_2 T^2$ term is due to electron–electron interaction, $\rho_{2.5} T^{2.5}$ term is due to electron–magnon interaction, $\rho_{4.5} T^{4.5}$ term is due to spin wave scattering process in the ferromagnetic region and $\rho_5 T^5$ term is the resistivity due to electron–phonon interaction.

The square of linear correlation coefficient (R^2) values were calculated for each equation and are listed in Table 4. Equation (13) is the most satisfied one in all samples (Table 4), and Fig. 7 shows the fitting of resistivity below T_{ms} with Eq. (13) for $x = 0.075$ as an example. Equation (13) emphasizes the presence of grain boundaries, electron–electron interaction, spin wave scattering and electron–phonon interaction, which play an essential role in conduction mechanism in the metallic region, and their coefficients generally increase with doping (Table 5), leading to an increase in resistivity. The large increase observed in all coefficients of $x = 0.075$ may be attributed to the completely orthorhombic transition that has high lattice distortion, and such high values were reported previously in Refs. [32, 51] for higher concentrations in the orthorhombic distortion.

Table 4 Square of linear correlation coefficient (R^2) values for equations in ferromagnetic region

x	$\rho = \rho_0 + \rho_2 T^2$	$\rho = \rho_0 + \rho_{2.5} T^{2.5}$	$\rho = \rho_0 + \rho_2 T^2 + \rho_{4.5} T^{4.5}$	$\rho = \rho_0 + \rho_2 T^2 + \rho_{4.5} T^{4.5} + \rho_5 T^5$
0	0.9871	0.9815	0.9913	0.9992
0.025	0.9848	0.9781	0.9933	0.9995
0.050	0.9750	0.9664	0.9962	0.9972
0.075	0.9636	0.9599	0.9973	0.9992

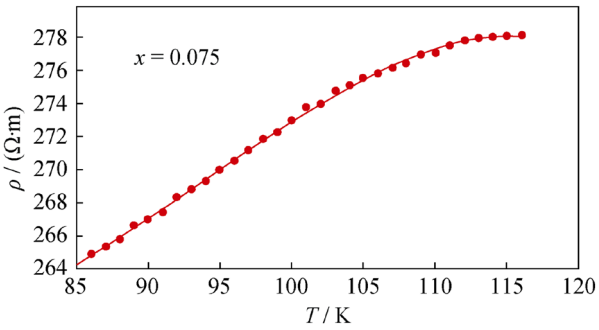

Fig. 7 Temperature-dependent resistivity of $x = 0.075$ below T_{ms}, solid line representing the best fitting with Eq. (13)

Table 5 Best-fitting parameters obtained from Eq. (13)

x	ρ_0	$\rho_2/10^{-4}$	$\rho_{4.5}$	$\rho_5/10^{-9}$
0	6.23	479.00	1.59×10^{-1}	1.12
0.025	9.01	4.96	1.63×10^{-8}	1.16
0.050	11.42	2.20	1.50×10^{-8}	1.00
0.075	265.29	57.00	31.2×10^{-8}	24.00

4 Conclusion

In this work, structural, magnetoresistive and electrical properties of LSMO doped with Ni^{2+} ($x = 0$, 0.025, 0.050 and 0.075) were investigated. This results in a decrease in the DE mechanism, which in turn decreases T_{ms} and increases resistivity with Ni^{2+} doping. The MR is enhanced with low doping of Ni^{2+} and decreases for high doping level.

Acknowledgments This work was financially supported by Sohag University in Egypt. The authors also would like to thank H F Mohamed for his continuous help.

References

[1] Reddy YS, Kistaiah P, Reddy CV. Elastic properties of double layered manganites $R_{1.2}Sr_{1.8}Mn_2O_7$. Rare Met. 2014;33(2):166.
[2] Asamitsu A, Moritomo Y, Kumai R, Tomioka Y, Tokura Y. Magnetostructural phase transitions in $La_{1-x}Sr_xMnO_3$ with controlled carrier density. Phys Rev B. 1996;54(3):1716.
[3] Helmolt RV, Wecker J, Holzapfel B, Schultz L, Samwer K. Giant negative magnetoresistance in perovskitelike $La_{2/3}Ba_{0.3}MnO_x$ ferromagnetic films. Phys Rev Lett. 1993;71(14):2331.
[4] Salamon MB, Jaime M. The physics of manganites: structure and transport. Rev Mod Phys. 2001;73(3):583.
[5] Kallel N, Dezanneau G, Dhahri J, Oumezzine M, Vincent H. Structure, magnetic and electrical behaviour of $La_{0.7}Sr_{0.3}Mn_{1-x}Ti_xO_3$ with $0 \le x \le 0.3$. J Magn Magn Mater. 2003;261(1–2):56.
[6] Kuharuangrong S, Dechakupt T, Aungkavattana P. Effects of Co and Fe addition on the properties of lanthanum strontium manganite. Mater Lett. 2004;58(12–13):1964.
[7] Zheng Y, Zhang C, Ran R, Cai R, Shao Z, Farrusseng D. A new symmetric solid-oxide fuel cell with $La_{0.8}Sr_{0.2}Sc_{0.2}Mn_{0.8}O_{3-\delta}$ perovskite oxide as both the anode and cathode. Acta Mater. 2009;57(4):1165.
[8] Jaime M, Salamon MB, Rubienstein M, Treece RE, Horwitz JS, Chrisey DB. High-temperature thermopower in $La_{2/3}Ca_{1/3}MnO_3$ films: evidence for polaronic transport. Phys Rev B. 1996;54(17):11914.
[9] Vanitha PV, Singh RS, Natarajan S, Rao CNR. Effect of substitution of Mn^{3+} by Ni^{3+} and Co^{3+} on the charge-ordered states of the rare earth manganates $Ln_{0.5}A_{0.5}MnO_3$. Solid State Commun. 1999;109(3):135.
[10] Righi L, Gorria P, Insausti M, Guiterrez J, Barandiaran JM. Influence of Fe in giant magnetoresistance ratio and magnetic properties of $La_{0.7}Ca_{0.3}Mn_{1-x}Fe_xO_3$ perovskite type compounds. J Appl Phys. 1997;81(8):5767.
[11] Zhang LW, Feng G, Liang H, Cao BS, Meihong Z, Zhao YG. The magnetotransport properties of $LaMn_{1-x}Cr_xO_3$ manganites. J Magn Magn Mater. 2000;219(2):236.
[12] Maignan A, Damay F, Barnabe A, Martin C, Hervieu M, Raveau B. The effect of Mn-site doping on the magnetotransport properties of CMR manganites. Phil Trans R Soc Lond A. 1998;356(1742):1635.
[13] Toulemonde O, Studer F, Raveau B. Magnetic interactions studies of Co and Ni-doped manganites using soft XMCD. Solid State Commun. 2002;118(2):107.
[14] Sanchez MC, Garcia J, Blasco J, Subias G, Cacho JP. Local electronic and geometrical structure of $LaNi_{1-x}Mn_xO_{3+\delta}$ perovskites determined by X-ray-absorption spectroscopy. Phys Rev B. 2002;65(14):144409.
[15] Gutierrez J, Pena A, Barandiaran JM, Pizarro JL, Lezama L, Insausti M, Rojo T. Structural, magnetic and magnetotransport properties of $La_{0.7}Pb_{0.3}Mn_{0.9}TM_{0.1}O_3$ (TM = Fe, Co, Ni) CMR perovskites. J Phys Condens Matter. 2000;12(50):10523.
[16] Hu J, Ji C, Qin H, Chen J, Hao Y, Li Y. Enhancement of room temperature magnetoresistance in $La_{0.65}Sr_{0.35}Mn_{1-x}T_xO_3$ (T = Fe and Ni) manganites. J Magn Magn Mater. 2002;241(2–3):271.
[17] Zener C. Interaction between the shells in the transition metals. Phys Rev. 1951;81:440.
[18] Park K. Fabrication and electrical properties of Mn–Ni–Co–Cu–Si oxides negative temperature coefficient thermistors. J Am Ceram Soc. 2005;88(4):862.
[19] Yonglai F, Ong CK. The magnetoresistance effect of La–Ca–Sr–Mn–O perovskites under a very low magnetic field. J Magn Magn Mater. 2000;208(1–2):69.
[20] Wandekar RV, Wani BN, Bharadwaj SR. Crystal structure, electrical conductivity, thermal expansion and compatibility studies of Co-substituted lanthanum strontium manganite system. Solid State Sci. 2009;11(1):240.
[21] Wandekar RV, Wani BN, Bharadwaj SR. Effect of Ni substitution on the crystal structure and thermal expansion behaviour of $(La_{0.8}Sr_{0.2})_{0.95}MnO_3$. Mater Lett. 2005;59(22):2799.
[22] Daengsakul S, Thomas C, Thomas I, Mongkolkachit C, Siri S, Amornkitbamrung V, Maensiri S. Magnetic and cytotoxicity properties of $La_{1-x}Sr_xMnO_3 (0 \le x \le 0.5)$ nanoparticles prepared by a simple thermal hydro-decomposition. Nano Scale Res Lett. 2009;4:839.
[23] Joshi L, Keshri S. Magneto-transport properties of Fe-doped LSMO manganites. Measurement. 2011;44(5):938.
[24] Hu XK, Xu MH, Wang ZS, Zhang SY, Wu Q, Si PZ. Magnetoresistance and magnetostriction effects in bulk Dy-doped $La_{2/3}Sr_{1/3}MnO_3$. Solid State Commun. 2009;149(5–6):243.
[25] Kuharuangrong S. Effects of Ni on the electrical conductivity and microstructure of $La_{0.82}Sr_{0.16}MnO_3$. Ceram Inter. 2004;30(2):273.
[26] Pal S, Bose E, Chaudhuri BK, Yang HD, Neeleshwar S, Chen YY. Effect of Ni doping in rare-earth manganite $La_{0.7}Pb_{0.3}Mn_{1-x}Ni_xO_3$ ($x = 0.0$–0.5). J Magn Magn Mater. 2005;293(2):872.

[27] Eshraghi M, Salamati H, Kameli P. The effect of NiO doping on the structure, magnetic and magnetotransport properties of $La_{0.8}Sr_{0.2}MnO_3$ composite. J Alloy Compd. 2007;437(1–2):22.
[28] Troyanchuk IO, Samsonenko NV, Nabiaiek A, Szymczak H. Magnetic interactions and phase transitions in the Co- and Ni-doped manganites. J Magn Magn Mater. 1997;168(3):309.
[29] Blasse G. Ferromagnetic interactions in non-metallic perovskites. J Phys Chem Solids. 1965;26(12):1969.
[30] Kallel N, Oumezzine M, Vincent H. Neutron-powder-diffraction study of structural and magnetic structure of $La_{0.7}Sr_{0.3}Mn_{1-x}Ti_xO_3$ ($x = 0$, 0.10, 0.20, and 0.30). J Magn Magn Mater. 2008;320(12):1810.
[31] Hwang HY, Palstra TTM, Cheong SW, Batlogg B. Pressure effects on the magnetoresistance in doped manganese perovskites. Phys Rev B. 1995;52(21):15046.
[32] Mostafa AG, Abdel-Khalek EK, Daoush WM, Moustfa SF. Study of some co-precipitated manganite perovskite samples-doped iron. J Magn Magn Mater. 2008;320(24):3356.
[33] Mahesh R, Mahendiran R, Raychaudhuri AK, Rao CNR. Effect of particle size on the giant magnetoresistance of $La_{0.7}Ca_{0.3}MnO_3$. Appl Phys Lett. 1996;68:2291.
[34] Roy B, Poddar A, Das S. Electrical transport properties and magnetic cluster glass behavior of $Nd_{0.7}Sr_{0.3}MnO_3$ nanoparticles. J Appl Phys. 2006;100(10):104318.
[35] Gupta A, Gong GQ, Xiao G, Lecoeur P, Trouilloud P, Wang YY, Dravid VP, Sun JZ. Grain-boundary effects on the magnetoresistance properties of perovskite manganite films. Phys Rev B. 1996;54(22):R15629.
[36] Dubourdieu C, Audier M, Senature JP, Pierre J. Effects of the microstructure on the magnetotransport properties of polycrystalline manganite films grown by metalorganic chemical vapor deposition. J Appl Phys. 1999;86(12):6945.
[37] Mathur ND, Burnell G, Isaac SP, Jackson TJ, Teo BS, Driscoll JLM, Cohen LF, Evetts JE, Blamire MG. Large low-field magnetoresistance in $La_{0.7}Ca_{0.3}MnO_3$ induced by artificial grain boundaries. Nature. 1997;387(6630):266.
[38] Hwang H, Cheong SW, Ong NP, Batlogg B. Spin-polarized intergrain tunneling in $La_{2/3}Sr_{1/3}MnO_3$. Phys Rev Lett. 1996; 77(10):2041.
[39] Ziese M, Srinitiwarawong C. Polaronic effects on the resistivity of manganite thin films. Phys Rev B. 1998;58(17):11519.
[40] Chen XJ, Zhang CL, Gardner JS, Sarrao JL, Almasan CC. Variable-range-hopping conductivity of the half-doped bilayer manganite $LaSr_2Mn_2O_7$. Phys Rev B. 2003;68:064405.
[41] Chen XJ, Zhang CL, Almasan CC, Gardner JS, Sarrao JL. Small-polaron hopping conduction in bilayer manganite $La_{1.2}Sr_{1.8}Mn_2O_7$. Phys Rev B. 2003;67(9):094426.
[42] Ramirez AP. Colossal magnetoresistance. J Phys Condens Matter. 1997;9:8171.
[43] Abdelmoula N, Rouhou AC, Reversat L. Structural, magnetic and magnetoresistive properties of $La_{0.7}Sr_{0.3-x}Na_xMnO_3$ manganites. J Phys Condens Matter. 2001;13(3):449.
[44] Mott NF, Davis EA. Electronics Process in Non Crystalline Materials. Oxford: Clarendon Press; 1979. 32.
[45] Austin IG, Mott NF. Polarons in crystalline and non-crystalline materials. Adv Phys. 1969;18(71):41.
[46] Mollah S, Huang HL, Yang HD, Pal S, Taran S, Chaudhuri BK. Non-adiabatic small-polaron hopping conduction in $Pr_{0.65}Ca_{0.35-x}Sr_xMnO_3$ perovskites above the metal–insulator transition temperature. J Magn Magn Mater. 2004;284:383.
[47] Pal S, Banerjee A, Rozenberg E, Chaudhuri BK. Polaron hopping conduction and thermoelectric power in $LaMnO_{3+\delta}$. J Appl Phys. 2001;89(9):4955.
[48] Viret M, Ranno L, Coey JMD. Magnetic localization in mixed-valence manganites. Phys Rev B. 1997;55(13):8067.
[49] Holstein T. Studies of polaron motion: part II. The "small" polaron. Ann Phys. 1959;8(3):343.
[50] Snyder GJ, Hiskes R, Dicarolis S, Beasley MR, Geballe TH. Intrinsic electrical transport and magnetic properties of $La_{0.67}Ca_{0.33}MnO_3$ and $La_{0.67}Sr_{0.33}MnO_3$ MOCVD thin films and bulk material. Phys Rev B. 1996;53(21):14434.
[51] Lakshmi YK, Venugopal RP. Influence of sintering temperature and oxygen stoichiometry on electrical transport properties of $La_{0.67}Na_{0.33}MnO_3$ manganite. J Alloy Compd. 2009; 470(1–2):67.